

Relativistic Cholesky-decomposed density matrix MP2

Benjamin Helmich-Paris,^{1,2,a)} Michal Repisky,³ and Lucas Visscher²

¹⁾*Max-Planck-Institut für Kohlenforschung, Kaiser-Wilhelm-Platz 1, D-45470 Mülheim an der Ruhr*

²⁾*Section of Theoretical Chemistry, Vrije Universiteit Amsterdam, De Boelelaan 1083, 1081 HV Amsterdam, The Netherlands*

³⁾*Hylleraas Centre for Quantum Molecular Sciences, Department of Chemistry, UiT The Arctic University of Norway, N-9037 Tromø Norway*

(Dated: 2 February 2022)

In the present article, we introduce the relativistic Cholesky-decomposed density (CDD) matrix second-order Møller–Plesset perturbation theory (MP2) energies. The working equations are formulated in terms of the usual intermediates of MP2 when employing the resolution-of-the-identity approximation (RI) for two-electron integrals. Those intermediates are obtained by substituting the occupied and virtual quaternion pseudo-density matrices of our previously proposed two-component atomic orbital-based MP2 (*J. Chem. Phys.* **145**, 014107 (2016)) by the corresponding pivoted quaternion Cholesky factors. While working within the Kramers-restricted formalism, we obtain a formal spin-orbit overhead of 16 and 28 for the Coulomb and exchange contribution to the 2C MP2 correlation energy, respectively, compared to a non-relativistic (NR) spin-free CDD-MP2 implementation. This compact quaternion formulation could also be easily explored in any other algorithm to compute the 2C MP2 energy. The quaternion Cholesky factors become sparse for large molecules and, with a block-wise screening, block sparse-matrix multiplication algorithm, we observed an effective quadratic scaling of the total wall time for heavy-element containing linear molecules with increasing system size. The total run time for both 1C and 2C calculations was dominated by the contraction to the exchange energy. We have also investigated a bulky Te-containing supramolecular complex. For such bulky, three-dimensionally extended molecules the present screening scheme has a much larger prefactor and is less effective.

I. INTRODUCTION

In recent years, quantum chemistry has made a substantial step forward in applying accurate wave function-based methods to large molecules and solids. Besides several flavours of fragment-based approaches,¹⁻⁵ in particular the revived pair-natural orbital approach of Neese and co-workers⁶⁻⁹ lead to efficient implementations that allowed coupled cluster energy calculation of molecules with hundreds of atoms — even proteins.^{8,9}

An alternative approach is to formulate the working equations completely in the atomic orbital (AO) basis by means of a Laplace transformation of the orbital energy denominator.¹⁰⁻¹⁵ In the AO basis all intermediates including the integrals become sparse for extended systems. By employing screening techniques that account for the rapid decay of the MP2 energy with respect to inter-electronic distances¹⁶⁻¹⁹ efficient implementations were presented by Ochsenfeld and his co-workers that allowed calculations on molecules with more than 2000 atoms and 20,000 basis functions.^{19,20} A reformulation in terms of AOs by means of Laplace and related transformations has also been pursued for properties and other electronic structure methods: MP2 analytic first-derivatives,^{21,22} MP2 nuclear magnetic shieldings,²³ explicitly correlated MP2-F12 energies,²⁴ periodic MP2 energies,²⁵ Dyson correction to quasi-particle energies,²⁶ CCSD energies,²⁷ perturbative triples correction (T) to CCSD,²⁸ direct random-phase approximation (dRPA) energies,^{29,30} and multi-reference second-order perturbation theory (NEVPT2).³¹ However, screening of intermediates in the AO basis has a substantial overhead compared to conventional molecular orbital (MO) implementations if large basis sets in combination with diffuse functions are used in the MP2 calculation. Those extended basis sets are necessary to describe dispersion interactions between non-covalently bonded molecules accurately, which is one of the target applications of MP2 and coupled cluster methods.

To reduce the pre-factor of AO-MP2, a pivoted Cholesky decomposition of AO density matrices has been proposed by the Ochsenfeld group. Those Cholesky-decomposed densities (CDD) can preserve the sparsity of the AO density matrices while reducing the rank, which is at most the number of active occupied or virtual orbitals. Consequently, CDD can be considered as generating localized molecular orbitals for the occupied and virtual orbital space. With a CDD-based MP2 calculations larger basis sets with diffuse functions should be feasible to describe also dispersion interactions in large supra-molecular complexes

accurately.

Recently, the relativistic two-component (2C) MP2 method based on Kramers-restricted formalism has been reformulated and implemented in the AO basis by the present authors. It was shown that the working equations of spin-free non-relativistic and 2C AO-MP2 differ merely by their algebra, i.e. real versus quaternion, respectively. The quaternion formulation results in a maximum reduction of the working equations if point-group symmetry is not considered. We could also show that the imaginary parts of the quaternion intermediates, which represent the spin-orbit (SO) contribution to the correlation energy, are much smaller in magnitude than the real part of the intermediates. With an implementation that screens both negligible contributions from spatially well separated orbitals and small SO contributions of light elements, all-electron 2C-MP2 calculations of large heavy-element containing molecules should be feasible.

In the present paper, we reformulate the relativistic 2C AO-MP2 in terms of quaternion Cholesky-decomposed densities to allow also calculations on larger molecules with larger basis sets. To reduce the overhead of an AO-MP2 calculation even further, we approximate the two-electron integrals by the resolution-of-the-identity approximation^{32,33} combined with attenuated Coulomb operators^{34,35} for a more compact local auxiliary basis. We show the performance of the implementation in terms of total wall time, scaling with respect to the system size, and errors introduced by screening for linear chains of Te-substituted polyethylene glycol oligomers. Our block-wise screening protocol seems to be less effective for bulky molecules.

II. THEORY AND IMPLEMENTATION

A. Relativistic two-component Laplace-transformed AO-MP2

In our previous work, we have introduced a formulation of relativistic 2C MP2 energies within the Kramers-restricted formalism solely in terms of scalar AO basis functions.³⁶ Our reformulation in the AO basis is based on the numerical integration of the Laplace transform

of orbital energy denominators,

$$\frac{1}{x} = \int_0^\infty \exp(-x t) dt \approx \sum_{z=1}^{n_z} \omega_z \exp(-x t_z) \quad (1)$$

$$x = \varepsilon_a - \varepsilon_i + \varepsilon_b - \varepsilon_j, \quad (2)$$

that contain orbital energies ε , in which the occupied orbitals are indexed with i, j and the virtual molecular orbitals (MO) or spinors are indexed with a, b . In the remainder of the present article, we will follow the Einstein summation convention. As for non-relativistic (NR) AO-MP2, the Laplace transformation in Eq. (1) allows us to compute the 2C Coulomb and exchange MP2 correlation energy contributions $e_J^{(z)}$ and $e_K^{(z)}$ at each quadrature point z ,

$$E_{\text{MP2}} = - \sum_{z=1}^{n_z} \left(e_J^{(z)} - e_K^{(z)} \right) \quad (3)$$

$$e_J^{(z)} = 2 \operatorname{Re} \left((\underline{\boldsymbol{\mu}} \bar{\boldsymbol{\nu}} | \kappa \lambda)^{(z)} \right) \operatorname{Re} \left((\mu \nu | \underline{\boldsymbol{\kappa}} \bar{\boldsymbol{\lambda}})^{(z)} \right) \quad (4)$$

$$e_K^{(z)} = \operatorname{Re} \left((\underline{\boldsymbol{\mu}} \bar{\boldsymbol{\nu}} | \underline{\boldsymbol{\kappa}} \bar{\boldsymbol{\lambda}})^{(z)} \right) (\kappa \nu | \mu \lambda) \quad (5)$$

from two-electron AO integrals $(\mu \nu | \kappa \lambda)$ that were transformed by occupied

$$\underline{\mathbf{P}} = \sqrt[4]{|\omega_z|} \mathbf{C}^o \times e^{+\varepsilon^o t_z} \times (\mathbf{C}^o)^H \quad (6)$$

$$= \sqrt[4]{|\omega_z|} e^{+t_z \mathbf{P} \times \mathbf{F}} \times \mathbf{P} \quad (7)$$

$$\mathbf{P} = \mathbf{C}^o \times (\mathbf{C}^o)^H \quad (8)$$

and virtual quaternion pseudo-density matrices

$$\bar{\mathbf{P}} = \sqrt[4]{|\omega_z|} \mathbf{C}^v \times e^{-\varepsilon^v t_z} \times (\mathbf{C}^v)^H \quad (9)$$

$$= \sqrt[4]{|\omega_z|} e^{-t_z \mathbf{Q} \times \mathbf{F}} \times \mathbf{Q} \quad (10)$$

$$\mathbf{Q} = \mathbf{C}^v \times (\mathbf{C}^v)^H. \quad (11)$$

The overlap charge distribution $\Omega_{\mu\nu}$ as it appears in two-electron AO integrals is transformed as follows:

$$\underline{\boldsymbol{\mu}} \bar{\boldsymbol{\nu}} = \Omega_{\underline{\boldsymbol{\mu}} \bar{\boldsymbol{\nu}}} = \underline{\mathbf{P}}_{\mu\mu'} \times \Omega_{\mu'\nu'} \times \bar{\mathbf{P}}_{\nu'\nu} \quad (12)$$

Note that in the equations above bold symbols indicate quaternions. The quaternion (pseudo-) density matrices in Eqs. (6) and (9) are computed from real orbital energies ε

and quaternion molecular orbitals,

$$\mathbf{C} = \mathbf{C}^0 + \check{i} \mathbf{C}^1 + \check{j} \mathbf{C}^2 + \check{k} \mathbf{C}^3 \quad (13)$$

$$\mathbf{C}^* = \mathbf{C}^0 - \check{i} \mathbf{C}^1 - \check{j} \mathbf{C}^2 - \check{k} \mathbf{C}^3 \quad (14)$$

$$\mathbf{C}^H = (\mathbf{C}^*)^T, \quad (15)$$

which are the solutions of Dirac-Hartree-Fock equations in the Kramers-restricted formalism with maximum time-reversal symmetry reduction.^{37,38} Note that o and v denote the active occupied and, respectively, virtual part of $\boldsymbol{\varepsilon}$ and \mathbf{C} . Alternatively, the occupied and virtual quaternion pseudo-density matrices can be computed from the quaternion AO Fock matrix \mathbf{F} and the quaternion occupied \mathbf{P} and virtual \mathbf{Q} density matrices, respectively, as given in Eqs. (7) and (10).

We chose \times to indicate a non-commutative quaternion multiplication for which the three imaginary units obey the following multiplication rules: $\check{i}^2 = \check{j}^2 = \check{k}^2 = \check{i}\check{j}\check{k} = -1$. For notational convenience, we have also used \times to indicate products of quaternions with real numbers. The equations presented in this section are completely equivalent to spin-free non-relativistic AO-MP2 iff we switch from quaternion to real algebra, i.e. omit all imaginary parts.

B. Relativistic two-component Laplace-transformed CDD-RI-MP2

The rationale behind a re-formulation in the AO basis is that by employing localized objects as AO basis functions the number of non-negligible contributions to the correlation energy should scale linearly with the system size for large molecules. In particular for MP2 screening of small contributions should be effective as E_{MP2} decays as $\mathcal{O}(R^{-6})$ with R being the distance between two well separated charge distributions.

Nevertheless, one-index transformations of two-electron integrals by AO density matrices in Eqs. (12) introduce a substantial computational overhead compared to conventional implementations, which first reduce the dimension by partial transformations to the occupied scalar or spinor MO basis. An established approximation to reduce the costs of both conventional and local implementations of MP2 is the resolution-of-the-identity (RI) approximation^{32,33} that decomposes the four-center AO integrals by a product of two- and

three-index intermediates:

$$(\mu\nu|\kappa\lambda) \approx B_{\mu\nu}^P B_{\kappa\lambda}^P \quad (16)$$

$$B_{\mu\nu}^P = (\mu\nu|Q) [\mathbf{V}^{-1/2}]_{PQ} \quad (17)$$

$$V_{PQ} = (P|Q) \quad (18)$$

In Eqs. (16) and (17) P and Q are real atom-centered auxiliary basis functions. The errors introduced by the RI approximation with a Coulomb metric (18) are usually less than $100 \mu\text{E}_\text{H}$ per atom if auxiliary basis sets are used that were optimized for a given orbital basis set.³⁹

The computational costs of the AO-MP2 can be reduced even further if the pseudo-density matrices are decomposed into their Cholesky factors.^{30,40,41} For 2C AO-MP2 the quaternion pseudo-density matrices should preferably be decomposed by quaternion pivoted Cholesky decomposition (CD)

$$\mathbf{P} = \mathbf{L} \times (\mathbf{L})^H \quad (19)$$

to preserve the quaternion structure. In Eq. (19) and in the following we assume that the Cholesky factors have been pivoted already, which destroys their triangular structure.⁴² As for the NR case, pivoted quaternion CD of sparse quaternion (pseudo-)density matrices results in sparse Cholesky factors \mathbf{L} , which is illustrated in Fig. 1. To maintain locality as much as possible,³⁰ the quaternion pseudo-density matrices are transformed into an orthogonal AO basis prior to CD:

$$\mathbf{S} = \mathbf{L}'(\mathbf{L}')^T \quad (20)$$

$$\tilde{\mathbf{P}} = (\mathbf{L}')^{-1} \times \mathbf{P} \times (\mathbf{L}')^{-1} = \tilde{\mathbf{L}} \times (\tilde{\mathbf{L}})^H \quad (21)$$

$$\mathbf{L} = \mathbf{L}' \times \tilde{\mathbf{L}} \quad (22)$$

We adjust the ordering procedure for the Cholesky factors of Kussmann et al.⁴³ for quaternions. The weighted mean index in Ref. 43 is computed from the norm of a quaternion and the same column permutations are performed for all four quaternion components.

The 2C-CDD-E_J is obtained if the quaternion pseudo-density matrices Eqs. (6) and (9)

are replaced by their corresponding quaternion Cholesky decomposition Eq. (19):

$$\begin{aligned}
e_J &= \text{Re}((\underline{\mu}\bar{\nu}|\kappa\lambda)) \text{Re}((\mu\nu|\underline{\kappa}\bar{\lambda})) \\
&= \text{Re}(\mathbf{L}_{\mu i} \times \mathbf{B}_{ia}^P \times \mathbf{L}_{\nu a}^* \times B_{\kappa\lambda}^P B_{\mu\nu}^Q \text{Re}(\mathbf{L}_{\kappa j} \times \mathbf{B}_{jb}^Q \times \mathbf{L}_{\lambda b}^*)) \\
&= \text{Re}(\mathbf{B}_{ia}^P \times \mathbf{L}_{\nu a}^* \times \mathbf{L}_{\mu i}) B_{\mu\nu}^Q \text{Re}(\mathbf{B}_{jb}^Q \times \mathbf{L}_{\lambda b}^* \times \mathbf{L}_{\kappa j}) B_{\kappa\lambda}^P \\
&= \text{Re}((\mathbf{B}_{ai}^P)^* \times \mathbf{B}_{ai}^Q) \text{Re}((\mathbf{B}_{bj}^Q)^* \times \mathbf{B}_{bj}^P) \tag{23}
\end{aligned}$$

$$= Z_{PQ} Z_{PQ} \tag{24}$$

with

$$\mathbf{B}_{ai}^P = \mathbf{L}_{\mu a}^* \times B_{\mu\nu}^P \times \mathbf{L}_{\nu i}. \tag{25}$$

In Eq. (23) we exploited that multiplication of a real number a and a quaternion \mathbf{b} is commutative,

$$[a, \mathbf{b}]_{\times} = a \times \mathbf{b} - \mathbf{b} \times a = 0, \tag{26}$$

and that the real part of multiple quaternion products is invariant under cyclic permutations:

$$\text{Re}(\mathbf{a} \times \mathbf{b} \times \mathbf{c}) = \text{Re}(\mathbf{b} \times \mathbf{c} \times \mathbf{a}) = \text{Re}(\mathbf{c} \times \mathbf{a} \times \mathbf{b}) \tag{27}$$

Similarly, we proceed with the exchange energy

$$\begin{aligned}
e_K &= \text{Re}((\underline{\mu}\bar{\nu}|\underline{\kappa}\bar{\lambda})) (\kappa\nu|\mu\lambda) \\
&= \text{Re}(\mathbf{L}_{\mu i} \times \mathbf{B}_{ia}^P \times \mathbf{L}_{\nu a}^* \times \mathbf{L}_{kj} \times \mathbf{B}_{jb}^P \times \mathbf{L}_{\lambda b}^*) B_{\kappa\nu}^Q B_{\mu\lambda}^Q \tag{28}
\end{aligned}$$

$$= \text{Re}((\mathbf{B}_{ai}^P)^* \times \mathbf{B}_{aj}^Q \times (\mathbf{B}_{bj}^P)^* \times \mathbf{B}_{bi}^Q) \tag{29}$$

The non-commutativity of the quaternion multiplication entails us on contracting either one occupied or one virtual index in a product of two B-intermediate tensors (25), which is not optimal for an implementation that aims for efficiency. Instead, we would like to contract over the auxiliary basis functions. This requires an order change in the quaternion multiplication, i.e. swapping the second and third term of Eq. (29). As quaternion multiplications are non-commutative, we have to add a commutator term when computing e_K :

$$\begin{aligned}
e_K &= \text{Re}((\mathbf{B}_{ai}^P)^* \times \mathbf{B}_{aj}^Q \times (\mathbf{B}_{bj}^P)^* \times \mathbf{B}_{bi}^Q) \\
&= \text{Re}((\mathbf{B}_{ai}^P)^* \times (\mathbf{B}_{bj}^P)^* \times \mathbf{B}_{aj}^Q \times \mathbf{B}_{bi}^Q) \\
&\quad - \text{Re}((\mathbf{B}_{ai}^P)^* \times [(\mathbf{B}_{bj}^P)^*, \mathbf{B}_{aj}^Q]_{\times} \times \mathbf{B}_{bi}^Q) \tag{30}
\end{aligned}$$

The commutator term leads to 12 additional matrix multiplications and additions, which is given below in a general form for reasons of notational convenience:

$$\begin{aligned}
\text{Re}(\mathbf{a}^* \times [\mathbf{c}^*, \mathbf{b}]_{\times} \times \mathbf{d}) = 2 & \left(a_1 c_1 (b_2 d_2 + b_3 d_3) + a_2 c_2 (b_3 d_3 + b_1 d_1) + a_3 c_3 (b_1 d_1 + b_2 d_2) \right. \\
& + a_0 c_1 (b_2 d_3 - b_3 d_2) - a_2 c_3 (b_1 d_0 + b_2 d_3) + a_3 c_2 (b_1 d_0 - b_3 d_2) \\
& + a_0 c_2 (b_3 d_1 - b_1 d_3) - a_3 c_1 (b_2 d_0 + b_3 d_1) + a_1 c_3 (b_2 d_0 - b_1 d_3) \\
& \left. + a_0 c_3 (b_1 d_2 - b_2 d_1) - a_1 c_2 (b_3 d_0 + b_1 d_2) + a_2 c_1 (b_3 d_0 - b_2 d_1) \right)
\end{aligned} \tag{31}$$

Our 2C CDD-MP2 formulation uses a pivoted quaternion CD of both occupied and virtual pseudo-density matrices. Alternatively, one could decompose only the occupied pseudo-density matrices to benefit from a rank reduction by using occupied Cholesky factors and the sparsity of the virtual pseudo-density matrices. Both approaches were advocated by Ochsenfeld and his co-workers and lead to successful nearly linearly scaling non-relativistic implementations for large system.^{30,44} The correctness of Eqs. (23) and (30) was confirmed by comparing the 2C-MP2 correlation energies of our CDD-based implementation with those from the Kramers-unrestricted RI-MP2 implementation⁴⁵ in Turbomole.

C. Implementation details

A reduction of the computational work is achieved by screening Cholesky factors and the three-index integrals when transforming the three-index integrals to the local CDD, i.e. pseudo-MO basis. We follow the recipe developed by Kussmann and Ochsenfeld⁴⁶ in which the Cholesky factors and three-index AO-integrals for a given auxiliary basis function shell are divided into blocks of a given target block size. Only those blocks that have a Frobenius norm larger than a user given sparse-matrix threshold T_{sparse} are processed further and stored in a block compressed sparse row format (BCSR) with variable block size. Before three-index integrals and Cholesky factors are screened and packed in blocked sparse matrices, the atoms of the molecule are re-ordered to minimize the band width of a connectivity matrix by the reverse Cuthill-McKee algorithm.^{46,47} When multiplying two sparse matrices we filter negligible elements on-the-fly.⁴⁸ After the multiplication, we inspect the product blocks and discard those for which the Frobenius norm is smaller than T_{sparse} .

In addition to pre-screening of small intermediates, significant computational savings can

be made if the Coulomb operator of the three- and two-index integrals is attenuated by the complementary error function,^{30,35,49}

$$(\mu\nu|\kappa\lambda) \approx (\mu\nu|P)_\omega (\tilde{V})_{PQ} (Q|\kappa\lambda)_\omega \quad (32)$$

$$\tilde{\mathbf{V}} = \mathbf{V}_\omega^{-1} \mathbf{V} \mathbf{V}_\omega^{-1} \quad (33)$$

$$(\mu\nu|P)_\omega = (\mu\nu|\frac{\text{erfc}(\omega r_{12})}{r_{12}}|P) \quad (34)$$

$$(P|Q)_\omega = (P|\frac{\text{erfc}(\omega r_{12})}{r_{12}}|Q), \quad (35)$$

which, essentially, removes the long-range tail of r_{12}^{-1} . If the damping frequency ω is chosen appropriately, the sparsity of the overlap metric $S_{PQ} = \int \int \chi_P(\mathbf{r}_1)\chi_Q(\mathbf{r}_2)d\mathbf{r}_1d\mathbf{r}_2$ is combined with the accuracy of the Coulomb metric \mathbf{V}_{PQ} . Benchmark calculations with CDD-dRPA showed that $\omega = 0.1$ introduces only mHartree deviations from the Coulomb metric results while speeding-up the calculation by a factor 10.³⁰

Our algorithm for computing the SO-CDD-MP2 energies is given in Fig. 2. First of all, $\underline{\mathbf{P}}$ and $\bar{\mathbf{P}}$ are computed either from quaternion MOs or complex spinors. The first are obtained by diagonalizing the quaternion Fock matrix in terms of quaternion algebra;^{37,38,50} the latter are solution of the complex Fock matrix (*vide infra*) which is usually more efficient as highly tuned linear algebra routines can be employed.⁵¹ Then, $\underline{\mathbf{L}}$ and $\bar{\mathbf{L}}$ are computed by a naive pivoted quaternion Cholesky decomposition. The outer loop for the integral transformation step runs over shells of auxiliary basis function rather than individual spherical Harmonic components. Also the screening procedure incorporated in the sparse matrix multiplication accounts for the degeneracy of auxiliary basis function shells to maintain rotational invariance of the MP2 energies. After the transformation of the AO integrals with the CDDs, \mathbf{I}_{ai}^P is resorted such that the auxiliary index is the leading index. Note that for large molecules each super block $[ai]$ usually has a different number of auxiliary basis functions that is much smaller than the total number of unscreened auxiliary basis functions of the molecule. To compute the B intermediates, the resorted integrals are transformed with the Cholesky factors of the intermediate $\tilde{\mathbf{V}}$. The Cholesky factorization has to be performed for each super block $[ai]$ as the resorted integrals have a different number of block specific auxiliary basis functions P_i . The Z intermediate in a selected auxiliary basis P_i is computed via a symmetric rank update of the B intermediate and than added to the Z-intermediate in the full auxiliary basis. The dot product of the Z intermediate gives the Coulomb MP2 energy for

each quadrature point z . The algorithm for the exchange part of the MP2 energy is similar to conventional RI-MP2 implementations^{32,33} though in our implementation the two outer loops run over virtual rather than occupied blocks for a more efficient parallelization and in order to keep all occupied block associated to at least a single virtual block in memory. Moreover, we exploit that E_K is invariant when permuting either the two occupied or the two virtual block indices.

If only the Coulomb MP2 energy is required, as in SOS-MP2⁵² or dRPA,^{29,30,53} it is more efficient to transform the square of \mathbf{I}_{ai}^P only once with $\tilde{\mathbf{V}}$ for every quadrature point. However, the time-determining step of our CDD-MP2 implementation is the exchange energy computation. By working with B intermediates rather than transformed integrals \mathbf{I}_{ai}^P we can avoid transformations with $\tilde{\mathbf{V}}$ in the most inner loop for the algorithm that computes E_K .

III. COMPUTATIONAL DETAILS

Our 1C- and 2C-CDD-MP2 implementation is integrated into a development version of the DIRAC program package⁵⁴ for relativistic calculations. The uncontracted Cartesian integrals for real large-component basis functions were computed with the InteRest library.⁵⁵ The exponents and weights of the numerical quadrature in Eq. (1) were obtained from the minimax algorithm^{56,57} that is available as public open-source library.⁵⁸

All 1C and 2C Hartree–Fock calculations were performed with Turbomole 7.2.^{59,60} For the 1C and 2C calculations, we used the dscf⁶¹ and ridft^{51,61–63} module, respectively. The relativistic SO calculations with ridft were performed with DLU approximation^{64,65} to the exact 2C core Hamiltonian.^{66–68} For all HF and MP2 calculations, we employed the cc-pVTZ orbital⁶⁹ and auxiliary basis set³⁹ for H and the 2p elements. For the 1C-ECP calculations, we used the cc-pVTZ-PP orbital⁷⁰ and auxiliary basis set⁷¹ in combination with an ECP that puts 28 electrons in the core. For the all-electron X2C calculations, we used the Dyall valence triple ζ orbital basis set for Te.⁷² The corresponding auxiliary basis set was automatically generated by the AutoAux module⁷³ of ORCA⁷⁴ and provided as supplementary material.*reference to be inserted in final version*

We employed the frozen-core approximation for the following atoms: the $1s^2$ electrons of C, N, and O; the $4s^2 4p^6$ electrons of Te in ECP calculations; the $[\text{Ar}]3d^{10} 4s^2 4p^6$ electrons of Te in all-electrons calculations. The frozen-core approximation for valence property

calculations was presumed when designing the basis sets that we have used.

The Te-PEG-n oligomers were optimized with the Turbomole 7.2^{59,60} using the PBE density functional^{75,76} with D3 dispersion correction,^{77,78} and the def2-SVP orbital and auxiliary basis set⁷⁹⁻⁸¹ in combination with an ECP with 28 core electrons.⁷⁰ Likewise, we have optimized the structure of the Te-containing supra-molecular complex. All structures are available as supplementary material.*reference to be inserted in final version*

Unless otherwise noted, we used a target block length of 32 and a conservative screening threshold $T_{\text{sparse}} = 10^{-8}$ for the CDD-MP2 calculations. Furthermore, we have used for the larger molecule calculations 10 quadrature points for the numeric integration and present results for quadrature point number 5. The frequency for the Coulomb-attenuated integrals was set to 0.1.

IV. RESULTS AND DISCUSSION

A. Error analysis for small molecules

The numerical errors of MP2 correlation energies introduced by our CDD implementation are caused by (1) the RI approximation, (2) the numerical integration of the Laplace transform, and (3) the neglect of blocks with a small norm in sparse intermediates. For calculations of small molecules with sufficiently accurate sparse-matrix thresholds T_{sparse} , nearly all blocks are kept with the pursued screening protocol. Thus, when investigating small molecules we focus on the errors that are caused by the RI approximation and the numerical integration only and set T_{sparse} to zero. For a supramolecular complex of two tellurazol oxide monomers the convergence of the MP2 interaction with respect to number of quadrature points is shown in Fig. 3 for the 1C-ECP, SF-X2C, and SO-X2C Hamiltonians. For all three Hamiltonians the errors in the MP2 interaction energy converge rapidly to zero. For the all-electron calculations we have used uncontracted basis sets due to technical limitations of the X2C implementation in the Dirac program package. Moreover, for those calculations all virtual orbitals with an orbital energy larger than 40 a. u. were frozen to facilitate the reference calculation with the conventional Dirac MP2 implementation.⁸² All-electron calculations usually feature a much larger ratio of the maximum to minimum orbital energy denominator ($R = \max(x)/\min(x)$) as given in the caption of Fig. 3, which

requires more quadrature points to reach the same accuracy by the minimax algorithm.^{56,57} This is exactly what can be observed in Fig. 3, though for the present example, only one or two additional quadrature points are sufficient to reach the same accuracy in the X2C and ECP calculation.

The HF and correlation energy contribution to the MP2 interaction energies of the two Tellurazol oxide monomers are compiled in Tab. I. Using the RI approximation leads to a slight overestimation of the interaction energy. Due to a relatively large automatically generated auxiliary basis set for Tellurium when employing the X2C Hamiltonian, the RI error of all-electron calculations is significantly smaller than the one of the ECP calculations. Nevertheless, the RI errors are satisfactory if one considers the inherent methodological error of the MP2 method. Eventually, the RI errors would also decrease when using larger auxiliary (and orbital) basis sets.

B. Performance for large linear molecules

We investigated the scaling with the system size (Fig. 4) of 1C and 2C CDD-MP2 for linear chains of Tellurium-substituted poly-ethylene glycol oligomers Te-PEG- n with $n = \{4, 8, 12, 16, 24, 32, 48, 64\}$. All calculations were performed in parallel with 16 threads on a Intel Haswell node. The largest 1C-ECP CDD-MP2 calculation ($n=64$) involved 9987 and 27208 spherical Harmonic orbital and auxiliary basis functions, respectively. For the largest X2C CDD-MP2 calculation ($n=32$) 9449 spherical Harmonic orbital and 41523 auxiliary basis functions were employed. For a single quadrature point, the largest 1C-ECP CDD-MP2 calculation ($n=64$) took approximately 10 hours; the largest X2C CDD-MP2 calculation ($n=32$) 3 days and 8 hours. The contraction to exchange energy is for the 1C-ECP and X2C calculation by far the most time-consuming step and takes approximately 57 and 96 % of the total run time, respectively. This is expected as the E_K contraction is the only computational step with a formal $\mathcal{O}(N^5)$ scaling if no blocks can be screened. Additionally, the E_K contraction has the largest formal spin-orbit overhead (28) of all computational steps. Therefore, almost the total computation time is spent on the 2C exchange contraction. Improvements on the performance of the exchange contraction could be attained by different integral decomposition techniques like the tensor hyper-contraction.⁸³ Those can eventually result in an $\mathcal{O}(N^4)$ -scaling implementation that offers the possibility to avoid the quaternion

commutator term.

For the timings of the 1C-ECP and X2C CDD-MP2 calculation we observe an effective quadratic scaling with respect to the number spherical Harmonic orbital basis functions — a measure of the size of a molecule. We expect a better scaling if we would run the calculations in serial as I/O of transformed three-index integrals and B intermediates has also a significant contribution to the timings, which is at the moment not parallelized by our shared-memory OpenMP parallelization. Eventually, linear scaling of nearly all computational resources should be observable since the average number of significant, unscreened sparse CDD blocks [ai] per auxiliary shell converges to a constant value in the asymptotic limit (Fig. 5). That number is for the 1C-ECP calculation roughly a factor of two smaller than for each quaternion unit in the X2C calculations. Compared to the 1C-ECP calculations, we need more orbital basis functions for the all-electron calculations and would expect a larger number of active blocks. However, we observe the opposite. It is the large number of steep s, p, and d short-range AOs in both the orbital and auxiliary Te basis set that leads to a much smaller number of CDD blocks [ai] for each quaternion unit.

The largest impact on the run time and accuracy of our CDD-MP2 implementation is the screening of sparse matrices. We have chosen a rather conservative sparse-matrix screening threshold of $T_{\text{sparse}} = 10^{-8}$. The relative errors in ppm for the linear Te-PEG-n oligomers are given in Fig. 6 and are always smaller than 10 ppm. Compared to the error introduced by the RI approximation, the truncation error is negligible. Note that we were not able to calculate the larger oligomers without screening due to the wall time limit on the compute cluster and limited hard disk size. The errors are increasing with the system size and converge to a finite value when increasing the system size. We note that looser screening threshold of $T_{\text{sparse}} = 10^{-5}$ and 10^{-6} lead to unacceptably large errors that can be attributed to the transformation with the inverse or inverse square root of the Coulomb metric V_{PQ} . A more compact local RI basis should allow for calculations with looser thresholds, which is at the moment not available.

C. Performance for large bulky molecules

We also investigated the performance of our CDD-MP2 implementation for a bulky molecule, i.e. a supramolecular complex of the Buckyball C_{60} bound to two four-membered

rings that are closed by strong Te-O non-covalent bonds (Fig. 7a).⁸⁴ Computing intermolecular interaction energies of supramolecular complexes with heavy elements are potential applications of our 2C CDD-MP2 and we would like to study the feasibility of such calculations.

For the 1C-ECP calculation, we show in Fig. 7b contour plots of occupied pseudo-density matrix, its pivoted Cholesky factor, and localized occupied molecular orbitals obtained from the Foster-Boys localization scheme.⁸⁵ In contrast to the larger linear Te-PEG-n chains (*vide supra*), both the occupied pseudo-density matrix and pivoted Cholesky factor (CDD) are dense and, thus, not suited for our block-wise screening procedure. We have also pursued a localization of the occupied and virtual molecular orbitals (LMO) by the Foster-Boys procedure that minimizes the orbital variance.⁸⁵ As can be seen from Fig. 7b those localized molecular orbitals can be much more compact than the CDD. Nevertheless, the current screening scheme based on the inspection of CDD / LMO blocks did not lead to any negligible contributions for such bulky molecule. This is not surprising if one considers the diameter of the molecular complex in Fig. 7a of about 21.1 Å. The 1C CDD-MP2/cc-pVTZ-PP calculation of that Te-containing complex required 5288 and 14056 orbital and auxiliary basis functions, respectively. We needed a similar number of basis functions (5027/13704) for the 1C-ECP CDD-MP2 calculation of Te-PEG-32. The length of that linear molecule is 148.7 Å. Such one-dimensional systems offer a much better possibility for as screening as whole CDD/LMO blocks can be easily discarded. A similar screening efficiency could also be achieved for bulky molecules if they have a diameter of e.g. 100 Å and more but this would exceed computing resources that are generally available.

At the moment, an obvious direction towards an improved performance for bulky molecules along present lines seems to be unclear. The orbital spread of LMOs could be improved by minimizing higher orders of the orbital variance.⁸⁶⁻⁸⁸ One could also consider to return to an AO-basis implementation that screens shell pairs based on (distance-dependent) pseudo Schwarz estimates.^{12,17,18} A combination with the RI approximation or an multipole expansion of the far-field Coulomb interaction⁸⁹ seem to be yet unexplored.

V. CONCLUSIONS

In the present article, we have introduced the relativistic Cholesky-decomposed density (CDD) matrix MP2. The working equations are formulated in terms of the usual intermediates of RI-MP2 and are obtained by substituting the occupied and virtual quaternion pseudo-density matrices of our previously proposed 2C AO-MP2 by the corresponding pivoted quaternion Cholesky factors. While working within the Kramers-restricted formalism, we obtain a formal spin-orbit overhead of 16 and 28 for the Coulomb and exchange contribution to the 2C MP2 correlation energy, respectively, compared to a non-relativistic spin-free CDD-MP2 implementation. This reduced spin-orbit overhead is a consequence of the quaternion algebra which could also be exploited for any other conventional or approximate algorithm for 2C MP2 energies. The errors that were introduced by the RI approximation and the numerical integration were investigated for a small Te-containing supramolecular complex and are negligible if the inherent methodological error of MP2 as well as the basis set incompleteness error are considered. The quaternion Cholesky factors become sparse for large linear systems and, by adapting the block-wise screening, block sparse-matrix multiplication algorithm of Ochsenfeld and co-workers,³⁰ we were able to compute 1C-ECP MP2 correlation energies for a linear Te-containing polyethylene glycol chain Te-PEG-64 with more than 400 atoms and roughly 10,000 orbital basis functions within 10 h by using 16 threads. The X2C all-electron MP2 calculation of the half-size chain (Te-PEG-32) needed roughly the same number of basis functions, but due to the spin-orbit overhead much longer 3 d and 8 h with 16 threads. The total run time for both 1C and 2C calculations was dominated by the contraction to the exchange energy. This computational step has still the original MP2 $\mathcal{O}(N^5)$ scaling if no blocks can be screened. For the linear chains we observed an effective quadratic scaling of the total wall time with the system size. We have also investigated a bulky Te-containing supramolecular complex. For such bulky, three-dimensionally extended molecules the present implementation is unfortunately less suited as the CDDs are dense. Improvements on the performance of 2C-MP2 energies calculation for large and bulky molecular systems will be investigated in the near future.

VI. ACKNOWLEDGMENTS

B. H.-P. acknowledges gratefully financial support from the German Research Foundation DFG (Grant No. HE 7427/1-1) and from the Netherlands Organisation for Scientific Research NWO by a Veni fellowship (Grant No. 722.016.011). M. R. acknowledges financial support by the Research Council of Norway through its Centres of Excellence scheme, project number 262695. Computer time at the Dutch national super computer Cartesius granted by the NWO is very much appreciated. B. H.-P. would like to thank Georgi L. Stoychev for discussions on automatized auxiliary basis sets and Florian Weigend and Uwe Huniar for providing generous support on 2C Hartree-Fock calculations with Turbomole.

VII. SUPPORTING INFORMATION

The corresponding auxiliary basis set of the Dyall valence triple ζ basis for Tellurium was obtained by an automated fitting procedure (AutoAux) that is available in the ORCA quantum chemistry package and is provided as supplementary material. Furthermore, all Cartesian coordinates of molecular structure used in the present article are made available.

REFERENCES

^aElectronic mail: helmichparis@kofo.mpg.de

¹Li, W.; Li, S. *J. Chem. Phys.* **2004**, *121*, 6649–6657.

²Friedrich, J.; Hanrath, M.; Dolg, M. *J. Chem. Phys.* **2007**, *126*, 154110.

³Ziółkowski, M.; Jansík, B.; Kjærgaard, T.; Jørgensen, P. *J. Chem. Phys.* **2010**, *133*, 014107.

⁴Rolik, Z.; Szegedy, L.; Ladjánszki, I.; Ladóczki, B.; Kállay, M. *J. Chem. Phys.* **2013**, *139*, 094105.

⁵Nagy, P. R.; Kállay, M. *J. Chem. Phys.* **2017**, *146*, 214106.

⁶Neese, F.; Hansen, A.; Liakos, D. G. *J. Chem. Phys.* **2009**, *131*, 064103.

⁷Neese, F.; Wennmo, F.; Hansen, A. *J. Chem. Phys.* **2009**, *130*, 114108.

⁸Riplinger, C.; Sandhoefer, B.; Hansen, A.; Neese, F. *J. Chem. Phys.* **2013**, *139*, 134101.

⁹Schwilk, M.; Ma, Q.; Köppl, C.; Werner, H.-J. *J. Chem. Theory Comput.* **2017**, *13*, 3650–3675.

- ¹⁰ Almlöf, J. *Chem. Phys. Lett.* **1991**, *181*, 319–320.
- ¹¹ Häser, M.; Almlöf, J. *J. Chem. Phys.* **1992**, *96*, 489–494.
- ¹² Häser, M. *Theor. Chem. Acc.* **1993**, *87*, 147–173.
- ¹³ Ayala, P. Y.; Scuseria, G. E. *J. Chem. Phys.* **1999**, *110*, 3660–3671.
- ¹⁴ Surján, P. R. *Chem. Phys. Lett.* **2005**, *406*, 318 – 320.
- ¹⁵ Kobayashi, M.; Nakai, H. *Chem. Phys. Lett.* **2006**, *420*, 250 – 255.
- ¹⁶ Lambrecht, D. S.; Ochsenfeld, C. *J. Chem. Phys.* **2005**, *123*, 184101.
- ¹⁷ Lambrecht, D. S.; Doser, B.; Ochsenfeld, C. *J. Chem. Phys.* **2005**, *123*, 184102.
- ¹⁸ Maurer, S. A.; Lambrecht, D. S.; Flaig, D.; Ochsenfeld, C. *J. Chem. Phys.* **2012**, *136*, 144107.
- ¹⁹ Maurer, S. A.; Lambrecht, D. S.; Kussmann, J.; Ochsenfeld, C. *J. Chem. Phys.* **2013**, *138*, 014101.
- ²⁰ Doser, B.; Lambrecht, D.; Kussmann, J.; Ochsenfeld, C. *J. Chem. Phys.* **2009**, *130*, 064107.
- ²¹ Schweizer, S.; Doser, B.; Ochsenfeld, C. *J. Chem. Phys.* **2008**, *128*.
- ²² Vogler, S.; Ludwig, M.; Maurer, M.; Ochsenfeld, C. *J. Chem. Phys.* **2017**, *147*, 024101.
- ²³ Maurer, M.; Ochsenfeld, C. *J. Chem. Phys.* **2013**, *138*, 174104.
- ²⁴ Hollman, D. S.; Wilke, J. J.; Schaefer, H. F. *J. Chem. Phys.* **2013**, *138*, 064107.
- ²⁵ Ayala, P. Y.; Kudin, K. N.; Scuseria, G. E. *J. Chem. Phys.* **2001**, *115*, 9698–9707.
- ²⁶ Pino, R.; Scuseria, G. E. *J. Chem. Phys.* **2004**, *121*, 2553–2557.
- ²⁷ Scuseria, G. E.; Ayala, P. Y. *J. Chem. Phys.* **1999**, *111*, 8330–8343.
- ²⁸ Constans, P.; Ayala, P. Y.; Scuseria, G. E. *J. Chem. Phys.* **2000**, *113*, 10451–10458.
- ²⁹ Schurkus, H. F.; Ochsenfeld, C. *J. Chem. Phys.* **2016**, *144*.
- ³⁰ Luenser, A.; Schurkus, H. F.; Ochsenfeld, C. *J. Chem. Theory Comput.* **2017**, *13*, 1647–1655.
- ³¹ Helmich-Paris, B.; Knecht, S. *J. Chem. Phys.* **2017**, *146*, 224101.
- ³² Feyereisen, M.; Fitzgerald, G.; Komornicki, A. *Chem. Phys. Lett.* **1993**, *208*, 359–363.
- ³³ Weigend, F.; Häser, M. *Theor. Chem. Acc.* **1997**, *97*, 331–340.
- ³⁴ Adamson, R. D.; Dombroski, J. P.; Gill, P. M. W. *J. Comput. Chem.* **1999**, *20*, 921–927.
- ³⁵ Jung, Y.; Sodt, A.; Gill, P. M. W.; Head-Gordon, M. *P. Natl. Acad. Sci. USA* **2005**, *102*, 6692–6697.
- ³⁶ Helmich-Paris, B.; Repisky, M.; Visscher, L. *J. Chem. Phys.* **2016**, *145*.
- ³⁷ Saue, T.; Fægri, K.; Helgaker, T.; Gropen, O. *Mol. Phys.* **1997**, *91*, 937–950.

- ³⁸Saue, T.; Jensen, H. J. A. *J. Chem. Phys.* **1999**, *111*, 6211–6222.
- ³⁹Weigend, F.; Köhn, A.; Hättig, C. *J. Chem. Phys.* **2002**, *116*, 3175–3183.
- ⁴⁰Zienau, J.; Clin, L.; Doser, B.; Ochsenfeld, C. *J. Chem. Phys.* **2009**, *130*, 204112.
- ⁴¹Maurer, S. A.; Clin, L.; Ochsenfeld, C. *J. Chem. Phys.* **2014**, *140*, 224112.
- ⁴²Higham, N. J. *WIREs Comput. Stat.* **2009**, *1*, 251–254.
- ⁴³Kusmann, J.; Luenser, A.; Beer, M.; Ochsenfeld, C. *J. Chem. Phys.* **2015**, *142*, 094101.
- ⁴⁴Maurer, S. A.; Kusmann, J.; Ochsenfeld, C. *J. Chem. Phys.* **2014**, *141*, 051106.
- ⁴⁵Bischoff, F. A.; Klopper, W. *J. Chem. Phys.* **2010**, *132*, 094108.
- ⁴⁶Kusmann, J.; Ochsenfeld, C. *J. Chem. Phys.* **2007**, *127*, 054103.
- ⁴⁷Cuthill, E.; McKee, J. Reducing the Bandwidth of Sparse Symmetric Matrices. Proceedings of the 1969 24th National Conference. New York, NY, USA, 1969; pp 157–172.
- ⁴⁸Borštnik, U.; VandeVondele, J.; Weber, V.; Hutter, J. *Parallel Comput.* **2014**, *40*, 47 – 58.
- ⁴⁹Jung, Y.; Shao, Y.; Head-Gordon, M. *J. Comput. Chem.* **2007**, *28*, 1953–1964.
- ⁵⁰Shiozaki, T. *Mol. Phys.* **2017**, *115*, 5–12.
- ⁵¹Armbruster, M. K.; Weigend, F.; van Wüllen, C.; Klopper, W. *Phys. Chem. Chem. Phys.* **2008**, *10*, 1748–1756.
- ⁵²Jung, Y.; Lochan, R. C.; Dutoi, A. D.; Head-Gordon, M. *J. Chem. Phys.* **2004**, *121*, 9793–9802.
- ⁵³Eshuis, H.; Yarkony, J.; Furche, F. *J. Chem. Phys.* **2010**, *132*, 234114.
- ⁵⁴DIRAC, a relativistic ab initio electronic structure program, Release DIRAC17 (2017), written by H. J. Aa. Jensen, R. Bast, T. Saue, and L. Visscher, with contributions from V. Bakken, K. G. Dylla, S. Dubillard, U. Ekström, E. Eliav, T. Enevoldsen, E. Faßhauer, T. Fleig, O. Fossgaard, A. S. P. Gomes, T. Helgaker, J. Henriksson, M. Iliaš, Ch. R. Jacob, S. Knecht, S. Komorovský, O. Kullie, J. K. Lærdahl, C. V. Larsen, Y. S. Lee, H. S. Nataraj, M. K. Nayak, P. Norman, G. Olejniczak, J. Olsen, Y. C. Park, J. K. Pedersen, M. Pernpointner, R. di Remigio, K. Ruud, P. Sałek, B. Schimmelpfennig, J. Sikkema, A. J. Thorvaldsen, J. Thyssen, J. van Stralen, S. Villaume, O. Visser, T. Winther, and S. Yamamoto (see <http://www.diracprogram.org>).
- ⁵⁵Repisky, M. 2013; InteRest 2.0, An integral program for relativistic quantum chemistry.
- ⁵⁶Takatsuka, A.; Ten-no, S.; Hackbusch, W. *J. Chem. Phys.* **2008**, *129*, 044112.
- ⁵⁷Helmich-Paris, B.; Visscher, L. *J. Comput. Phys.* **2016**, *321*, 927 – 931.

- ⁵⁸Helmich-Paris, B. 2017; laplace-minimax library release v1.5 available from <https://github.com/bhelmichparis/laplace-minimax.git>.
- ⁵⁹TURBOMOLE V7.2 2017, a development of University of Karlsruhe and Forschungszentrum Karlsruhe GmbH, 1989-2007, TURBOMOLE GmbH, since 2007; available from <http://www.turbomole.com>.
- ⁶⁰Furche, F.; Ahlrichs, R.; Hättig, C.; Klopper, W.; Sierka, M.; Weigend, F. *WIREs Comput. Mol. Sci.* **2014**, *4*, 91–100.
- ⁶¹Häser, M.; Ahlrichs, R. *J. Comput. Chem.* **1989**, *10*, 104–111.
- ⁶²von Arnim, M.; Ahlrichs, R. *J. Comput. Chem.* **1998**, *19*, 1746–1757.
- ⁶³Ahlrichs, R. *Phys. Chem. Chem. Phys.* **2004**, *6*, 5119–5121.
- ⁶⁴Peng, D.; Reiher, M. *J. Chem. Phys.* **2012**, *136*, 244108.
- ⁶⁵Peng, D.; Middendorf, N.; Weigend, F.; Reiher, M. *J. Chem. Phys.* **2013**, *138*.
- ⁶⁶Iliáš, M.; Jensen, H. J. A.; Kellö, V.; Roos, B. O.; Urban, M. *Chem. Phys. Lett.* **2005**, *408*, 210 – 215.
- ⁶⁷Kutzelnigg, W.; Liu, W. *J. Chem. Phys.* **2005**, *123*, 241102.
- ⁶⁸Kutzelnigg, W.; Liu, W. *Mol. Phys.* **2006**, *104*, 2225–2240.
- ⁶⁹Dunning, T. H. *J. Chem. Phys.* **1989**, *90*, 1007–1023.
- ⁷⁰Peterson, K. A.; Figgen, D.; Goll, E.; Stoll, H.; Dolg, M. *J. Chem. Phys.* **2003**, *119*, 11113–11123.
- ⁷¹Hättig, C.; Schmitz, G.; Koßmann, J. *Phys. Chem. Chem. Phys.* **2012**, *14*, 6549–6555.
- ⁷²Dyall, K. G. *Theor. Chem. Acc.* **2006**, *115*, 441–447.
- ⁷³Stoychev, G. L.; Auer, A. A.; Neese, F. *J. Chem. Theory Comput.* **2017**, *13*, 554–562.
- ⁷⁴Neese, F. *WIREs Comput. Mol. Sci.* **2012**, *2*, 73–78.
- ⁷⁵Perdew, J. P.; Ernzerhof, M.; Burke, K. *J. Chem. Phys.* **1996**, *105*, 9982–9985.
- ⁷⁶Treutler, O.; Ahlrichs, R. *J. Chem. Phys.* **1995**, *102*, 346–354.
- ⁷⁷Grimme, S. *J. Comput. Chem.* **2006**, *27*, 1787–1799.
- ⁷⁸Grimme, S.; Antony, J.; Ehrlich, S.; Krieg, H. *J. Chem. Phys.* **2010**, *132*.
- ⁷⁹Schäfer, A.; Horn, H.; Ahlrichs, R. *J. Chem. Phys.* **1992**, *97*, 2571–2577.
- ⁸⁰Weigend, F.; Ahlrichs, R. *Phys. Chem. Chem. Phys.* **2005**, *7*, 3297–3305.
- ⁸¹Weigend, F. *Phys. Chem. Chem. Phys.* **2006**, *8*, 1057–1065.
- ⁸²Laerdahl, J. K.; Saue, T.; Fægri Jr., K. *Theor. Chem. Acc.* **1997**, *97*, 177–184.
- ⁸³Hohenstein, E. G.; Parrish, R. M.; Martínez, T. J. *J. Chem. Phys.* **2012**, *137*, 044103.

- ⁸⁴Ho, P. C.; Szydłowski, P.; Sinclair, J.; Elder, P. J. W.; Kübel, J.; Gendy, C.; Lee, L. M.; Jenkins, H.; Britten, J. F.; Morim, D. R.; Vargas-Baca, I. *Nat. Commun.* **2016**, *7*, 11299.
- ⁸⁵Foster, J. M.; Boys, S. F. *Rev. Mod. Phys.* **1960**, *32*, 300–302.
- ⁸⁶Jansík, B.; Høst, S.; Kristensen, K.; Jørgensen, P. *J. Chem. Phys.* **2011**, *134*, 194104.
- ⁸⁷Høyvik, I.-M.; Jansík, B.; Jørgensen, P. *J. Chem. Phys.* **2012**, *137*, 224114.
- ⁸⁸Høyvik, I.-M.; Jansík, B.; Jørgensen, P. *J. Chem. Theory Comput.* **2012**, *8*, 3137–3146.
- ⁸⁹White, C. A.; Johnson, B. G.; Gill, P. M.; Head-Gordon, M. *Chem. Phys. Lett.* **1994**, *230*, 8 – 16.

FIGURES

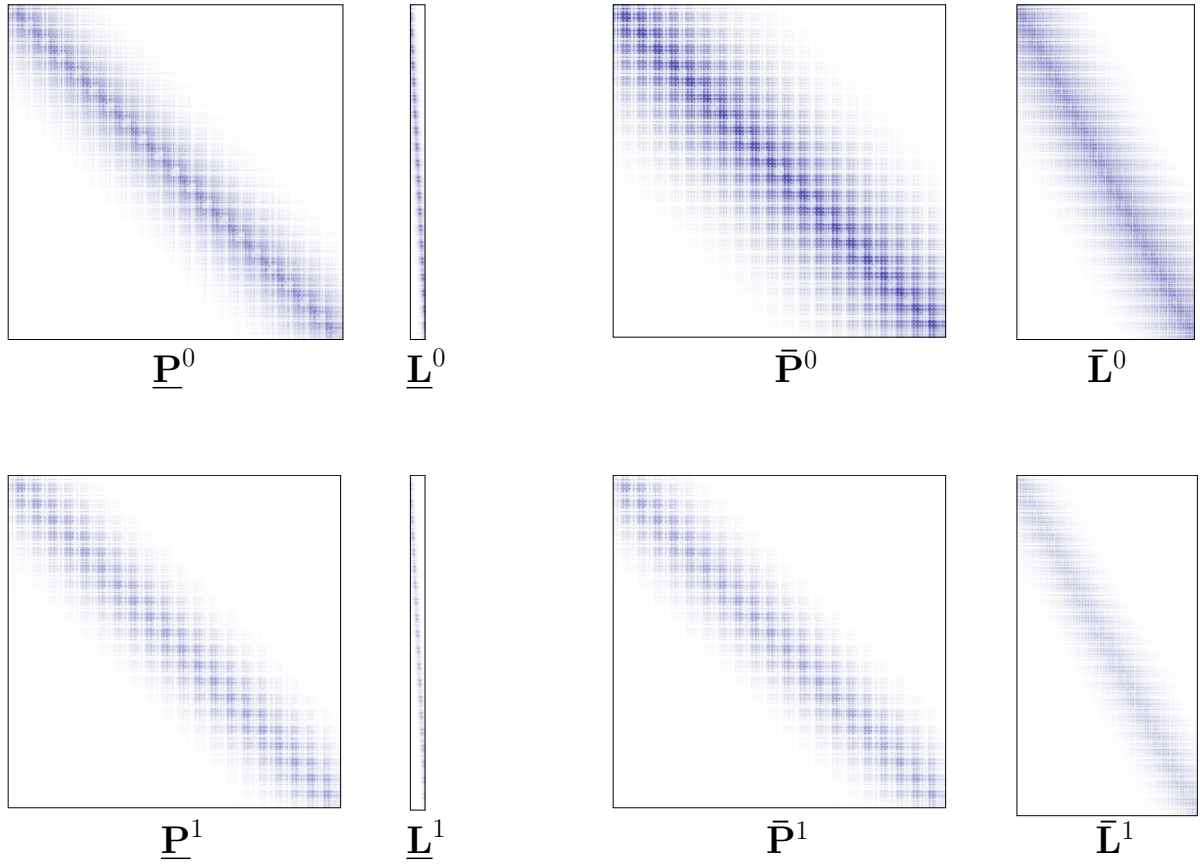


FIG. 1: Real (0) and first imaginary part (1) of the occupied and virtual quaternion pseudo-density matrix and pivoted quaternion Cholesky factors of Te-PEG-20.

compute pseudo-density matrices $\underline{\mathbf{P}}$ and $\bar{\mathbf{P}}$ and BCSR packing

CDD $\underline{\mathbf{L}}$ and $(\bar{\mathbf{L}})^H$ and BCSR packing

Schwarz estimates $Q_{\mu\nu,\omega} = \sqrt{(\mu\nu|\mu\nu)_\omega}$ and BCSR packing

integral transformation

for all auxiliary shells **do**

compute all $(\mu\nu|P)_\omega \forall \mu, \nu : Q_{\mu\nu} \geq T_{\text{Sparse}}$

for all z **do**

BCSR quaternion multiplication: $\mathbf{I}_{\mu i}^P = (\mu\nu|P)_\omega \times \underline{\mathbf{L}}_{\nu i}$

BCSR quaternion multiplication: $\mathbf{I}_{a i}^P = \bar{\mathbf{L}}_{a\mu}^* \times \mathbf{I}_{\mu i}^P$

write sparse matrices $\mathbf{I}_{a i}^P \forall P \in \text{aux. shell}$ to disk

resort $\mathbf{I}_{a i}^P$ and make P leading index

compute $\tilde{\mathbf{V}} = \mathbf{V}_\omega^{-1} \mathbf{V} \mathbf{V}_\omega^{-1}$

for all z **do**

for all super blocks $[ai]$ **do**

for all q **do**

read $\mathbf{I}_{a i}^P$

get subset of $\tilde{\mathbf{V}}_{P_i Q_i}$ for subset of aux. BF P_i part of $[ai]$

Cholesky decomposition: $\tilde{\mathbf{V}}_{P_i Q_i} = L_{P_i, \tilde{P}_i} L_{Q_i, \tilde{P}_i}$

$B_{a i}^{\tilde{P}_i, q} = L_{P_i, \tilde{P}_i} I_{a i}^{P_i, q}$

$Z_{\tilde{P}_i \tilde{Q}_i} = B_{a i}^{\tilde{P}_i, q} B_{a i}^{\tilde{Q}_i, q}$

$Z_{PQ+} = Z_{\tilde{P}_i \tilde{Q}_i}$

$e_J^{(z)+} = \text{tr}[\mathbf{Z}^T \mathbf{Z}]$

for all z **do**

for all batch of $[a]$ **do**

read \mathbf{B}_{a*}^P

for all batches of $[b]$ **do**

read \mathbf{B}_{b*}^P

for all $[a]$ **do**

for all $[b] \leq [a]$ **do**

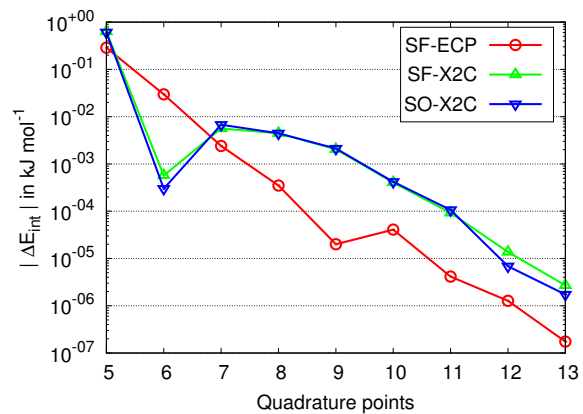
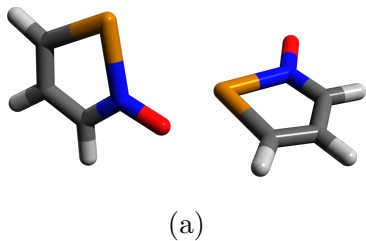
for all $[i]$ **do**

for all $[j] \leq [i]$ **do**

find common set of aux. BF for $[ai]$ and $[bj]$

$$e_K^{(z)} + = B_{ai}^P B_{bj}^P B_{aj}^Q B_{bi}^Q \text{ according to Eq. (30)}$$

FIG. 2: CDD-MP2 algorithm



(b)

FIG. 3: Convergence of the interaction energy errors of complex (a) with respect to the number of quadrature points for numerical integration of the Laplace transform (b). The fitting interval ratio for the minimax algorithm for the monomer (M) and dimer (D) are 1C-ECP: 498. (M), 661. (D); SF-X2C: 764. (M), 1620. (D); SO-X2C: 764. (M) and 1635. (D).

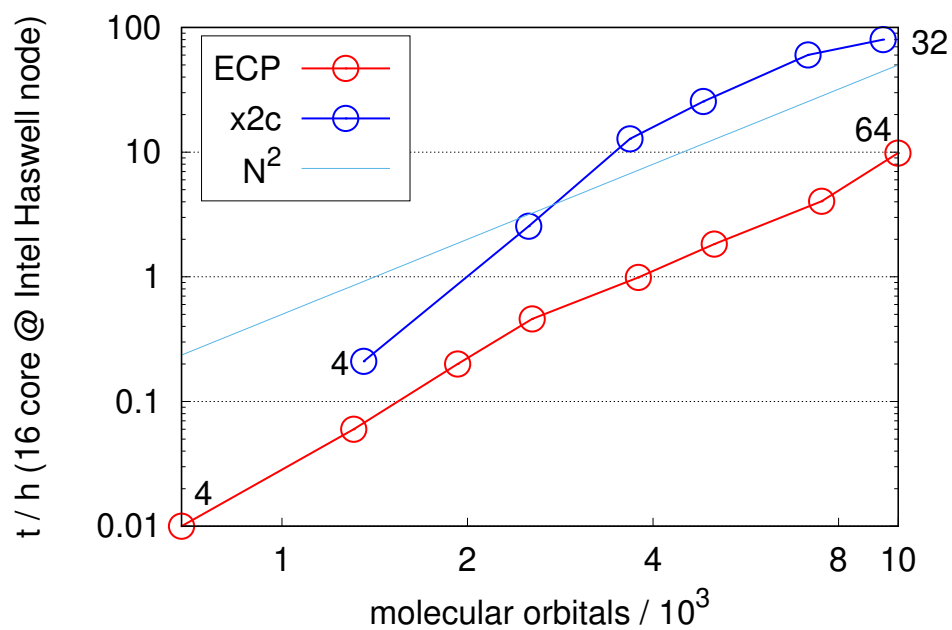


FIG. 4: Wall time of 1C-ECP and X2C CDD-MP2 calculations on Te-PEG- n with $n = \{4, 8, 12, 16, 24, 32, 48, 64\}$ for a single quadrature point on a single Intel Haswell node with 16 threads.

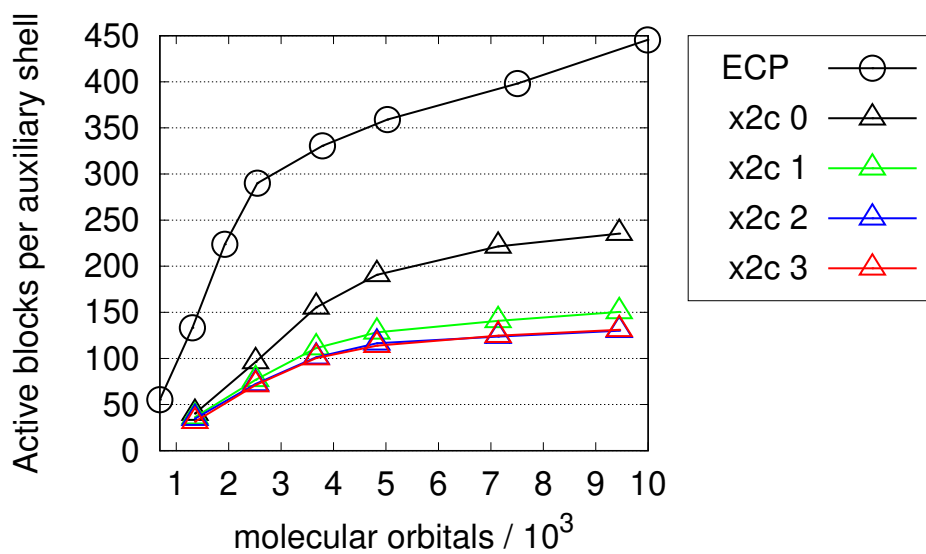


FIG. 5: Average number of active blocks per auxiliary basis function shell for 1C-ECP and X2C calculations on Te-PEG-n with $n = \{4, 8, 12, 16, 24, 32, 48, 64\}$.

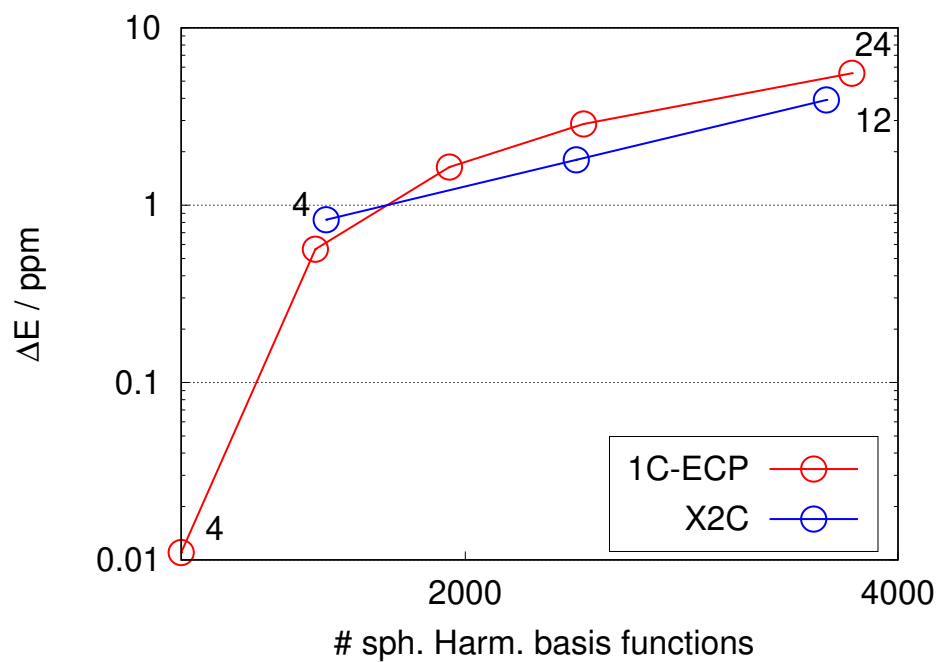


FIG. 6: Relative errors in ppm for 1C-ECP and X2C calculations on Te-PEG- n with $n = \{4, 8, 12, 16, 24, 32, 48, 64\}$.

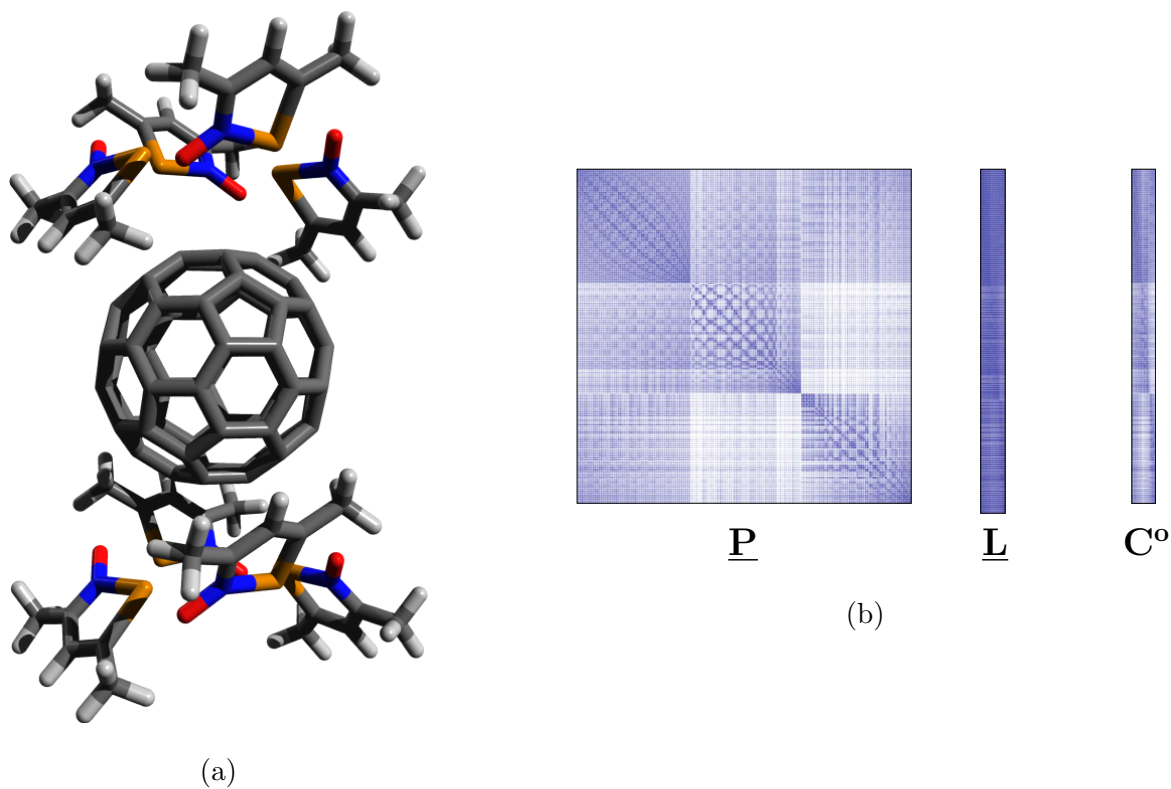


FIG. 7: A Te-containing supramolecular complex (a) with non-relativistic occupied pseudo-density matrix, pivoted Cholesky factors, and localized occupied molecular orbitals (b).

TABLES

TABLE I: Interaction energies of two tellurazol oxide molecules given in kJ mol^{-1} .

Hamiltonian	HF	RI-MP2 (corr.)	MP2 (corr.)	Δ RI
1C-ECP	-62.6831	-8.3451	-8.2763	-0.0688
SF-X2C	-61.6723	-9.9347	-9.9223	-0.0124
SO-X2C	-60.2273	-10.2285	-10.2205	-0.0080